USGS
science for a changing world

Geologic and Geophysical Data for Wells Drilled at Raft River Valley, Cassia County, Idaho, in 1977–1978 and Data for Wells Drilled Previously

By Manuel Nathenson, Thomas C. Urban, and Harry R. Covington

Open-File Report 2014–1201

U.S. Department of the Interior
U.S. Geological Survey

U.S. Department of the Interior
SALLY JEWELL, Secretary

U.S. Geological Survey
Suzette M. Kimball, Acting Director

U.S. Geological Survey, Reston, Virginia: 2014

For product and ordering information:
World Wide Web: http://www.usgs.gov/pubprod
Telephone: 1-888-ASK-USGS

For more information on the USGS—the Federal source for science about the Earth,
its natural and living resources, natural hazards, and the environment:
World Wide Web: http://www.usgs.gov
Telephone: 1-888-ASK-USGS

Suggested citation:
Nathenson, M., Urban, T.C., and Covington, H.R., 2014, Geologic and geophysical data for wells drilled at Raft River Valley, Cassia County, Idaho, in 1977–1978 and data for wells drilled previously: U.S. Geological Survey Open-File Report 2014-1201, 30 p., http://dx.doi.org/10.3133/ofr20141201.

ISSN 2331-1258 (online)

Contents

Figures

Tables

Conversion Factors

[Inch/Pound to SI]

Multiply	By	To obtain
foot (ft)	0.3048	meter (m)

Temperature in degrees Celsius (°C) may be converted to degrees Fahrenheit (°F) as follows:
°F=(1.8×°C)+32
Vertical coordinate information is referenced to the North American Datum of 1927 (NAD 27).
Horizontal coordinate information is referenced to the North American Datum of 1927 (NAD 27).
Altitude, as used in this report, refers to distance above the vertical datum.

Geologic and Geophysical Data for Wells Drilled at Raft River Valley, Cassia County, Idaho, in 1977–1978 and Data for Wells Drilled Previously

By Manuel Nathenson, Thomas C. Urban, and Harry R. Covington

Abstract

In order to better define the size of the thermal anomaly in the Raft River Valley, Idaho, the U.S. Geological Survey drilled a series of intermediate-depth (nominal 500-ft depth) wells in 1977 and 1978. This report presents geologic, geophysical, and temperature data for these drill holes, along with data for five wells drilled by the Idaho National Engineering Laboratory with U.S. Department of Energy funding. Data previously reported for other drill holes are also included in order to make them available as digital files.

For purposes of defining the thermal anomaly for the geothermal system, temperature gradients are calculated over long depth intervals on the basis of the appearance of reasonably linear segments on a temperature versus depth plot. Temperature versus depth data for some drill holes can be represented by a single gradient, whereas others require multiple gradients to match the data. Data for some drill holes clearly reflect vertical flows of water in the formation surrounding the drill holes, and water velocities are calculated for these drill holes. Within The Narrows area, temperature versus depth data show reversals at different depths in different drill holes. In the main thermal area, temperatures in intermediate-depth drill holes vary approximately linearly but with very high values of temperature gradient. Temperature gradients on a map of the area can be reasonably divided into a large area of regional gradients and smaller areas defining the thermal anomalies.

Introduction

The Idaho geothermal project was started in 1973 under Aerojet Nuclear Company at the National Reactor Testing Station with funding from the U.S. Atomic Energy Commission (Kunze and Miller, 1974). The purpose of the project was to develop the geothermal resource in the Raft River Valley for the generation of electricity. U.S. Geological Survey (USGS) investigators did earth science studies of geology, geophysics, hydrology, and water chemistry and drilled auger holes and intermediate-depth core holes. Work continued on the project at the renamed Idaho National Engineering Laboratory with funding from successor agencies: the Energy Research and Development Administration and then the U.S. Department of Energy. Results of the earth science studies were reported in Williams and others (1976), Mabey and others (1978), Ackermann (1979), Keys and Sullivan (1979), Nathenson and others (1980, 1982), and Urban and others (1986). Seven deep production and injection wells were drilled (Dolenc and others, 1981), and a 5-megawatt electric binary-cycle power plant was installed and

operated in 1981 and 1982 and shut down in 1982 (Bleim, 1983). The property was acquired by U.S. Geothermal in 2002, and a 13-megawatt power plant was constructed and brought on line in 2007 (Bradford and others, 2013).

In order to better define the size of the thermal anomaly, the USGS drilled a series of intermediate-depth wells in 1977 and 1978 with funding from the USGS Geothermal Research Program. The wells were completed with cemented casing in order to prevent water flows within the drill holes. Because data for the wells have not been previously published, this report now presents geologic, geophysical, and temperature data for these drill holes. In addition, data not previously published are reported for five wells drilled by the Idaho National Engineering Laboratory with U.S. Department of Energy funding. Data for wells previously reported by Urban and others (1986) are also included in order to make them available now in digital form. This report contains a summary discussion of the data, and the complete data files are included as appendixes. The data from all wells are used to define the areas of thermal anomalies.

Methods

The twenty-four wells designated the H series were drilled to 80 feet with a diameter of $7^7/_8$ inch using a rotary drilling rig. Welded casing 5 inches in diameter was placed in the well. Cement was mixed onsite, pumped down the casing, and followed by a wiper plug and water. The casing plug was drilled out with 4½-inch-diameter drill bit, and drilling was continued to a nominal 500 feet (fig. 1). Drill cuttings were collected every 5 feet and used to develop lithologic logs. Geophysical logs were run using one tool for caliper and resistivity and a second tool for natural gamma ray, with the data recorded on chart paper. Resistivity logs were calibrated using a calibration box, and caliper logs with a jig at 4, 6, and 8 inches to hold the caliper arms. Gamma ray logs were recorded as counts per second, with a calibration recorded at 200 American Petroleum Institute (API) units. All logs on chart paper were digitized at a later date. The resistivity logs were digitized using an arbitrary100-count scale along with the nonlinear resistance calibration recorded on the same scale. The resistance calibration is in ohms, and the relation of the resistance in ohms to the formation resistivity in ohm meters is unknown. After logging was completed, threaded casing of 2-inch diameter was placed in the hole with joint compound on the threads. Cement was pumped down the casing followed by a latching wiper plug and water. Drill hole H06 did not have 2-inch casing installed because it became artesian, and well H41 did not have 2-inch casing installed because time ran out at the end of the drilling program. Inclinometer measurements were made at discrete depths using hydrofluoric acid in small test tubes and are reported in appendix A.

Methods of measuring temperature versus depth evolved over the time period of logging wells at Raft River. The earliest measurements were made by stopping at discrete depths and recording the resistance of the thermistor attached to a four-conductor cable. The next step was logging at a fixed speed (fig. 2), with resistances recorded at specified depths using a teletype with paper tape. The final configuration was logging at a fixed speed with resistances converted to temperature in a Tektronix® 4051 computer and recorded on paper tape. Plots of temperature versus depth show the recorded data points as individual points. Further details of logging methods and calibration are given in Urban and others (1987). For wells that had pressure at the wellhead, pipes and a packing gland were added to keep the well from flowing (fig. 3).

Drill Hole Data

Locations of wells with data reported in this study are shown in figure 4, and location, depth, and drilling-date information are given in table 1, with letter codes for the location data in figure 5. Data for these wells, along with data for the auger holes reported in Urban (1986), are given in the appendixes. Wells drilled for this study are the H series, and the wells contracted by the Idaho National Engineering Laboratory are the HF series. Additional wells listed are those drilled earlier by the USGS (Crosthwaite, 1976), the deep wells in the RRGE series, and various other wells drilled by others that we were allowed to make temperature measurements in.

Geologic and geophysical data were collected along with temperature logs to select appropriate depths for measurement of thermal conductivity. Although we were not able to measure thermal conductivities, it is worth exploring detailed relationships between lithology and geophysical logs, and figure 6 shows these data for well H04. The lithology is sedimentary, with layers of siltstone, claystone, and conglomerate. The natural gamma-ray and resistance logs have a fair amount of variation, with layers of high and low values in each. There is no obvious relation between the lithologic character of the cuttings and the natural gamma-ray and resistance logs. The relation between the natural gamma-ray and resistance logs appears to change below a depth of around 450 ft. Above this depth, they seem to vary independently, whereas below this depth they appear to track together in that an increase (or decrease) in the values for one corresponds to an increase (or decrease) in the other. The temperature gradient values systematically decrease from ~80 °C/km to ~60 °C/km from a depth of about 90 ft to 300 ft. Such a systematic decrease is not reflected in any trend in either the lithology or the geophysical logs, and it most likely reflects vertical flow of water in the surrounding rocks (see discussion below). Below 450-ft depth, there are alternating layers of high and low temperature gradient values. There does seem to be a correspondence between the alternating layers in the temperature gradient values and changes in the geophysical log values. If one were sampling for thermal conductivity measurements, these alternating layers would be worth sampling to check whether the heat flow is constant through this lower part of the section. The upper 300 ft, with its water flow, would not be very good for assessing the deeper heat flow.

The theory for the effect of a vertical flow of water on temperatures was developed by Bredehoeft and Papadopulos (1965). For a layer with a temperature T_0 at the top and T_L at the bottom with water flowing at velocity v downwards, the temperature distribution is:

$$\frac{T - T_0}{T_L - T_0} = [\exp(\frac{\beta z}{L}) - 1] / [\exp(\beta) - 1] \quad (1a)$$

$$\beta = \rho_w c_w v L/k \quad (1b)$$

where z is depth, ρ_w and c_w are, respectively, the density and specific heat of water, L is the length of the layer, and k is the thermal conductivity of the formation. Differentiating this result, the temperature gradient is:

$$\frac{dT}{dz} = (T_L - T_0)\frac{\beta}{L}\exp(\frac{\beta z}{L})/[\exp(\beta) - 1]. \quad (2)$$

Thus, plotting the temperature gradient on a log scale versus a linear scale for depth results in straight-line behavior. The temperature gradient for well H04 is a linear function of depth on a

log scale from about 93 to 295 ft, with some variation about this linear dependence (fig. 6). The estimated velocity is –0.026 m/y. The curvature in the profile (fig. 7) is not large, but for other wells discussed below, it is much stronger, and their flow velocities are larger in magnitude (table 2).

Thermal conductivities were measured for a number of wells at Raft River (table 3), and the data are plotted in Nathenson and others (1980) and Urban and others (1986). Measurements were done using the needle-probe technique, which tends to result in significant scatter in values (Urban and others, 1986). This is reflected in the large values for the standard deviation given in table 3, a better measure of the uncertainty than the standard error (the large number of measurements results in small values that are misleading). Despite the large uncertainties, a considerable range in values for thermal conductivity is evident from the four wells. Well I.D. 5 has a significant amount of quartz monzonite in brecciated blocks or as part of conglomerate (Crosthwaite, 1976; H.R. Covington, written commun., 1977). Temperatures for well I.D. 5A (near I.D. 5 but deeper) are given in figure 10, and there are two zones of differing gradients. Heat flows calculated with the two gradients and average thermal conductivities differ by 10 percent (table 3). Thermal conductivities in the three other wells are significantly lower. Because these three wells are in the thermal area (see below), the temperature gradients and heat flows have a wide range and cannot be used to judge whether one value of thermal conductivity is more representative of the sediments in the valley than another. Urban and others (1986) chose amongst the values in table 3 to calculate heat flows for other wells, but we shall use temperature gradients instead.

Although the detailed variations discussed above are interesting, they are not very helpful without measurements of thermal conductivity. For purposes of defining the thermal anomaly for the geothermal system, we will focus on temperature gradients calculated over longer depth intervals based on the appearance of reasonably linear segments chosen by eye on a temperature versus depth plot. Figure 7 shows the selected temperature gradients in well H04. The temperature gradients over long depth intervals miss the detailed variations in figure 6, but they are reasonably representative.

Estimates of such representative gradients are provided in table 4 and shown on a map of drill hole locations in figure 8. The temperature versus depth data for some drill holes are reasonably represented by a single gradient, whereas others require two gradients. The map showing temperature gradients can be reasonably divided into a large area of regional gradients and smaller areas defining the thermal anomalies. The thermal anomalies are defined as having a temperature gradient >70 °C/km. The basis for the contours is further developed in the next section. The area of the main thermal anomaly is shown open towards the Jim Sage Mountains, as no thermal data constrain its extent in that direction. The thermal anomaly at Almo 1 is shown as a small area also open towards the Jim Sage Mountains.

Temperatures in Drill Holes by Area

Figure 9 repeats the temperature gradients from figure 8 and outlines areas with the figure numbers for the following plots of temperature versus depth. Figure 10 shows data for I.D. 5A and other drill holes in the northwest part of the Raft River Valley. Well I.D. 5 was drilled to a depth of 718 ft to measure regional heat flow (Nathenson and others, 1980), and well I.D. 5A was drilled nearby to a depth of 1,197 ft to assess if the temperature gradient continued to greater depth. The gradients from 500 ft to total depth are 44.2 °C/km in I.D. 5 and 44.9 °C/km in I.D.

5A, essentially the same. Drill hole H05 has a somewhat erratic profile, but the overall gradient of 56 °C/km (table 4) is somewhat less than the upper gradient of 64 °C/km in I.D. 5A. The bottom section of H05 has a gradient of 176 °C/km from 488 to 500 ft, and this very high gradient probably reflects a water flow. Drill hole H03 has an irregular temperature versus depth profile, with three reasonably linear sections (table 4) and a nonlinear section at about 300-ft depth. Temperature gradients in the upper part of the profile are 56 and 70 °C/km, but from 440 to 508 ft, the gradient is 95 °C/km. This latter gradient is similar to the gradient in drill hole H07 of 89 °C/km, which is clearly much steeper than the other drill holes in this group (fig. 10). Drill hole H04 (fig. 7, discussed above) has an upper gradient of 72 °C/km and a deeper gradient of 53 °C/km. Drill hole H08 has a gradient of 65°C/km. Comparing the temperature versus depth plots for the various drill holes in figure 10, some of the temperature gradients are quite variable, but the temperatures at a given depth group reasonably together. Drill hole H07 is clearly warmer, with a consistent gradient of 89 °C/km, and appears to define the boundary of the thermal anomaly. The gradients for well H06 are also high (table 4), but the well is shallow, has only surface casing, and is under artesian pressure. The well is in a saddle between the Jim Sage Mountains and Sheep Mountain just to the east, and the gradients are assumed to be influenced by hydrology. The Jim Sage Mountains are to the west of these drill holes (fig. 9), and there is significant topographic relief to drive water flows in the subsurface. Some of the changes in temperature gradient could well be related to horizontal flows of water, and the temperatures in well H04 demonstrate vertical flow of water.

Drill holes in the eastern part of the Raft River Valley (fig. 9) are generally cool (fig. 11*A*) and define the eastern extent of the thermal anomaly. Well H15 has a low gradient of 45 °C/km. Well H17 has two gradients of 43 and 66 °C/km, and the latter gradient is similar to the gradient of 68 °C/km in well H18. The temperatures in H17 and H18 are similar (fig. 11*A*). Wells H01 and H16 have strongly nonlinear temperature gradients (fig. 11*B*). This behavior reflects vertical flow of water downward in the surrounding rock as indicated by straight-line variation with depth of the log of the temperature gradient (fig. 11*B*). The straight-line fits to the log of the temperature gradient versus depth (fig. 11*B*) are pretty good matches. The velocity of water flow is 0.12 m/y in H01 and 0.072 m/y in H16 (downward). This would indicate groundwater recharge in the vicinity of the wells.

Although it does not appear that the wells are deep enough to get beyond the downward water flow, estimates of overall gradients are obtained by taking a temperature at depth where the straight-line behavior starts and a temperature at the total depth of the wells. These estimated gradients are 46 °C/km in H01 and 43 °C/km in H16, and the values are shown on figures 8 and 9. The overall temperature gradients in these wells are quite similar to that in H15 of 45 °C/km.

The reasons for the variations about the straight-line behavior of the log of the temperature gradients for wells H01 and H16 (fig. 11*B*) are not clear. For well H01, most but not all of the variations in gradient shown in figure 11*B* also occur when plotting temperature gradients from the temperature log of July 30, 1979 (not shown). Thus the variations in gradient either reflect some variation with depth in the thermal regime in the surrounding rock or some variation caused by the influence of the drill hole completion. Although the casing was cemented from bottom to top, we have no measures to demonstrate that the cement prevents small flows of water over short distances. The casing joints used were 21 ft in length, and the wavelength of some of the anomalies are of that order. For some of the variations in well H01, the gradient first increases and then decreases with increasing depth. This is not to be expected if there were enhanced downward flow, and this behavior may indicate a small upward flow imposed on the

temperature profile for downward flow in the formation. Given that these drill holes were completed using methods designed for high-quality measurements of temperature versus depth, these unexplained variations, noticeable because of the high precision of the temperature measurements, may reflect our inability to stop small variations caused by imperfect drill hole completion.

Temperature gradients in the area just to the north of the deep wells RRGE 1, 2, and 3 (fig. 9) are significantly higher than those in areas farther north and to the east. Temperature gradients are 89 °C/km in H07 and 88 and 78 °C/km in upper and lower parts of H02. Temperatures are higher in wells HF1 and HF2 (fig. 12), as are the temperature gradients (fig. 9). The temperature profiles in HF1 and HF2 may reflect water flows within the annulus between the casing and drill hole, because cement was probably added only from above. Well I.D. 1 has rather variable temperature gradients but becomes warmer than H02 and H07 below 350 ft. Notable but small jumps in temperature in well H02 occur at depths of 288, 330, 372, and 414 ft. In each case, the difference in depth between the jumps is 42 ft or two casing lengths. The calibrated inclinometer angle from vertical is 4.8° at 260 ft, 9.5° at 360 ft, and 7.9° at 460 ft, and it seems likely that the sinker bar above the temperature probe was sliding along the casing. It would appear that the sinker bar was slightly hanging up at some of the casing joints, reducing the tension in the cable, and then being released from the impediment and falling and retensioning the cable to rapidly increase the temperature. However, the temperature jumps range from 0.1 to 0.14 °C. The amount that would happen from lowering the cable along the temperature gradient by 2 ft is 0.05 °C, and the extra temperature increase represents the probe dropping an additional 2 to 4 feet. The amount of slack before the cable goes completely slack in the logging truck at these depths in 2-in casing is probably only 2 feet and may not be as large as 4 ft.

Temperature gradients in the area of the deep wells RRGE 1, 2, and 3 (fig. 9) are quite high. The highest temperatures are in Shuter's Hot Well (SHW), reaching nearly 94 °C at 402 ft (fig. 13). Well H09, about 3,000 ft northwest and about 100 ft higher in elevation, has a somewhat lower gradient, and temperatures reach 44.4 °C at 548 ft. Similar to Shuter's Hot Well, H09 has nearly isothermal temperatures in the bottom part of the well. Wells I.D. 2 and I.D. 3 also have high gradients (fig. 9) and temperatures (fig. 13). To the southeast, well HF3 has a lower gradient and well H14 has a gradient that is approximately regional in value (56 °C/km).

Temperatures in The Narrows area (fig. 14*A*) show the effect of horizontal flow of warm water. Well I.D. 4 has a temperature of 42.5 °C at 80 ft. The form of the profile indicates that either the flow of warm water started at a relatively recent time (see, for example, Ziagos and Blackwell, 1986) or that the flow overlies a flow of cooler water to explain the temperature reversal. Auger Hole A.H. 13-N is about 500 ft north of wells H10 and H30 and has a temperature of 78.3 °C at a depth of 51 ft. Wells H10 and H30 are immediately adjacent to each other. Well H30 was drilled to try to get below the temperature reversal, but the reversal continued to total depth of 898 ft. The temperature profiles in H10 and H30 are broadly similar. The maximum temperature in H10 is 67.1 °C at a depth of 325 ft, and that in H30 is 71.5 °C at a depth of 364 ft. The reason for the difference in temperature and depth of maximum temperature is unclear. The upper part of the profile in H30 suggests water flows from incompletely cemented casing. Both wells intercept rhyolite lava flows below 260 ft. The varying depths and values of maximum temperatures indicate that the fluid-flow system is quite complex.

Temperatures for the cooler wells in The Narrows are shown in figure 14*B*, along with temperature gradients for H11 and H12 on a log scale. The temperature gradient in the upper part

of H12 is 171 °C/km. The lower part has an upward flow of water as shown by the curvature in the temperature versus depth plot (fig. 14*B*), and the plot of the log of the temperature gradient versus depth is linear from 195 to 517 ft, confirming this behavior. The vertical velocity is –0.13 m/y (upwards). The temperature gradient in the lower part of H12 is 75 °C/km. Well H35 has a temperature gradient of 164 °C/km. Temperatures in H12 and H35 are similar, though H35 is hotter near its bottom. Representative temperature gradients in the middle and lower parts of H11 are 120 and 100 °C/km, respectively. The temperature profile in well H11 shows both a downflow of water in its middle part and an upflow in its lower part (fig. 14*B*). The velocity in the upper part of H11 is 0.094 m/y and in the lower part –0.23 m/y. Thus the upward flow in the bottom part of H11 and the downward flow in the middle depth range exit at a depth of around 400 ft and become a horizontal flow of water. This depth coincides with the bottom of the brecciated zone at the top of the rhyolite lava flow (fig. A-46) and with the depth where resistance and natural gamma-ray values increase (fig. A-48). Well H13 has temperature gradients of 48 and 97 °C/km in the middle and lower parts, respectively, and an overall gradient of 73 °C/km. Temperatures in H11 and H13 are less than in H35 and H12, and the lower temperatures in these wells reflect the approach to regional temperature gradients away from the thermal anomaly (fig. 8).

Wells HF4 and HF5 are between The Narrows and the deep wells RRGE 1, 2, and 3, and figure 15 shows data for them along with data for H12. Wells HF4 and H12 have similar temperatures in their upper parts, though both have upward flows of water and lower temperature gradients in their deeper parts. Well HF5 is between these two wells and has lower temperatures and temperature gradients (80, 109 °C/km). The cooler behavior of HF 5 suggests a separation between the system found in the deep wells and the system found in The Narrows area.

Data for wells in the Upper Raft River Valley are given in figure 16. Almo 1 is an artesian well. Although temperatures in Almo 1 were measured through a packing gland, the high temperature at the surface indicates that the temperatures are probably still disturbed from previous episodes of flow. The maximum temperature in the well is 73.6 °C at a depth of 484 ft, indicating the presence of flowing thermal water in the formation. The other wells are significantly cooler, with the warmest being H35 on one edge of the thermal anomaly in The Narrows. Almo 2, to the west of Almo 1, has a gradient of 50 °C/km, similar to regional values in other wells. Well H21 to the south has gradients of 52 and 89 °C/km in its upper and lower parts, respectively, but its temperatures are not particularly high. Well H19 has a gradient of 53 °C/km in its middle part, with a very low gradient below. The general behavior of the wells surrounding Almo 1 indicates that the thermal anomaly is relatively local but open towards the Jim Sage Mountains.

Conclusions

Combining data for the wells drilled as part of this study with those previously drilled allows better definition of the thermal anomalies in the Raft River area. A somewhat surprising finding is that many wells are affected by vertical water flows in the formation even when not within the active hydrothermal system. Obtaining quality temperature gradients in the sediments of the Raft River Valley was difficult, though it was possible to obtain reasonably representative temperature gradients in many wells. Some of the variations in temperature gradient are probably due to variations in thermal conductivities, but thermal conductivity data are lacking.

Acknowledgments

The drill rig was contracted with Western Geophysical of Bakersfield, California, and the driller was Rod Lund, with helpers Greg Dean and Jerry Bainbridge. Mark Bond and Bennie Loebner provided field assistance during the drilling. Urban and Nathenson supervised the drilling and conducted the logging. Covington did the lithologic descriptions. Marianne Guffanti provided field assistance during the 1979 logging. Patrick Muffler and Steve Ingebritsen are thanked for helpful reviews.

References Cited

Ackermann, H.D., 1979, Seismic refraction study of the Raft River geothermal area, Idaho: Geophysics, v. 44, p. 216–225.

Bleim, C.J., Jr., 1983, The Raft River 5MW(e) binary geothermal-electric power plant—Operation and performance: Geothermal Resources Council Transactions, v. 7, p. 3–13.

Bradford, J., McLennan, J., Moore, J., Glasby, D., Waters, D., Kruwell, R., Bailey, A., Rickard, W., Bloomfield, K., and King, D., 2013, Recent developments at the Raft River geothermal field: Proceedings Thirty-Eighth Workshop on Geothermal Reservoir Engineering, Stanford University, February 10–13, 2013, SGP-TR-198, 10 p., accessed May 17, 2013, at https://pangea.stanford.edu/ERE/pdf/IGAstandard/SGW/2013/2013program.html.

Bredehoeft, J.D., and Papadopulos, I.S., 1965, Rates of vertical groundwater movement estimated from the Earth's thermal profile: Water Resources Research, v. 1, p. 325–328.

Crosthwaite, E.G., 1976, Basic data from five core holes in the Raft River geothermal area, Cassia County, Idaho: U.S. Geological Survey Open-File Report 76-665, 12 p., 5 plates.

Dolenc, M.R., Hull, L.C., Mizell, S.A., Russell, B.F., Skiba, P.A., Strawn, J.A., and Tullis, J.A., 1981, Raft River geoscience case study: Idaho National Engineering Laboratory, EG&G Idaho, Inc., EGG-2125, v. 1, 145 p., accessed May 17, 2013, at http://www.osti.gov/energycitations/product.biblio.jsp?query_id=2&page=0&osti_id=6098820.

Keys, W.S., and Sullivan, J.K., 1979, Role of borehole geophysics in defining the physical characteristics of the Raft River geothermal reservoir, Idaho: Geophysics, v. 44, p. 1116–1141.

Kunze, J.F., and Miller, L.G., 1974, Idaho geothermal R & D project report for period December 16, 1973 to March 15, 1974: Aerojet Nuclear Company ANCR-1115, 38 p., accessed August 5, 2014, at http://www.osti.gov/geothermal/purl.cover.jsp?purl=/4279469-trYhrr/.

Mabey, D.R., Hoover, D.B., O'Donnell, J.E., and Wilson, C.W., 1978, Reconnaissance geophysical studies of the geothermal system in southern Raft River Valley, Idaho: Geophysics, v. 43, p. 1470–1484.

Nathenson, M., Urban, T.C., Diment, W.H., and Nehring, N.L., 1980, Temperatures, heat flow, and water chemistry from drill holes in the Raft River geothermal system, Cassia County, Idaho: U.S. Geological Survey Open-File Report 80–2001, 30 p.

Nathenson, M., Nehring, N.L., Crosthwaite, E.G., Harmon, R.S., Janik, C., and Borthwick, J., 1982, Chemical and light-stable isotope characteristics of waters from the Raft River geothermal area and environs, Cassia County, Idaho; Box Elder County, Utah: Geothermics, v. 11, p. 215–237.

Urban, T.C., Diment, W.H., Nathenson, M., Smith, E.P., Ziagos, J.P., and Shaeffer, M.H., 1986, Temperature, thermal-conductivity, and heat-flux data; Raft River area, Cassia County, Idaho (1974–1976): U.S. Geological Survey Open-File Report 86–123, 299 p.

Urban, T.C., Diment, W.H., and Sorey, M.L., 1987, Temperatures and natural gamma-ray logs obtained in 1986 from Shady Rest drill hole RD08, Mammoth Lakes, Mono County, California: U.S. Geological Survey Open-File Report 87–291, 100 p.

Williams, P.L., Covington, H.R., and Pierce, K.L., 1982, Cenozoic stratigraphy and tectonic evolution of the Raft River basin, Idaho, *in* Bonnichsen, B., and Breckenridge, R.M., eds., Cenozoic geology of Idaho: Idaho Bureau of Mines and Geology Bulletin 26, p. 491–504.

Williams, P.L., Mabey, D.R., Zohdy, A.A.R., Ackerman, H., Hoover, D.B., Pierce, K.L., and Oriel, S.S., 1976, Geology and geophysics of the southern Raft River Valley geothermal area, Idaho, U.S.A.: Proceedings, Second United Nations Symposium on the Development and Use of Geothermal Resources, San Francisco, Calif., 1975, v. 2, p. 1273–1282.

Ziagos, J.P., and Blackwell, D.D., 1986, A model for the transient temperature effects of horizontal fluid flow in geothermal systems: Journal of Volcanology and Geothermal Research, v. 27, p. 371–397.

Figure 1. Photograph of drilling rig on well H01 with 4 ½-inch diameter drill bit (August 21, 1977).

Figure 2. Photograph of logging truck with cable in well (1979).

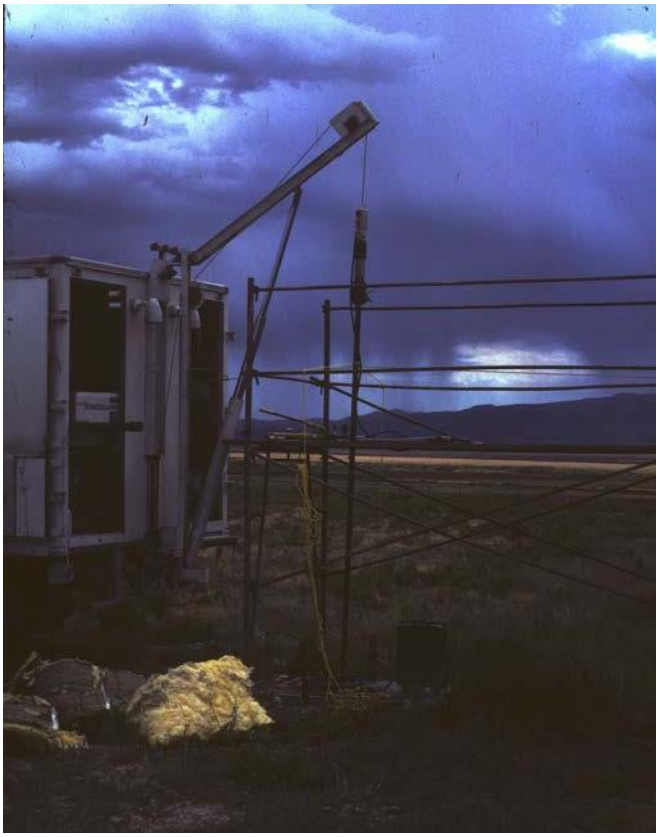

Figure 3. Photograph showing logging of well I.D.3 with stand pipe and packing gland on top (August 11, 1976).

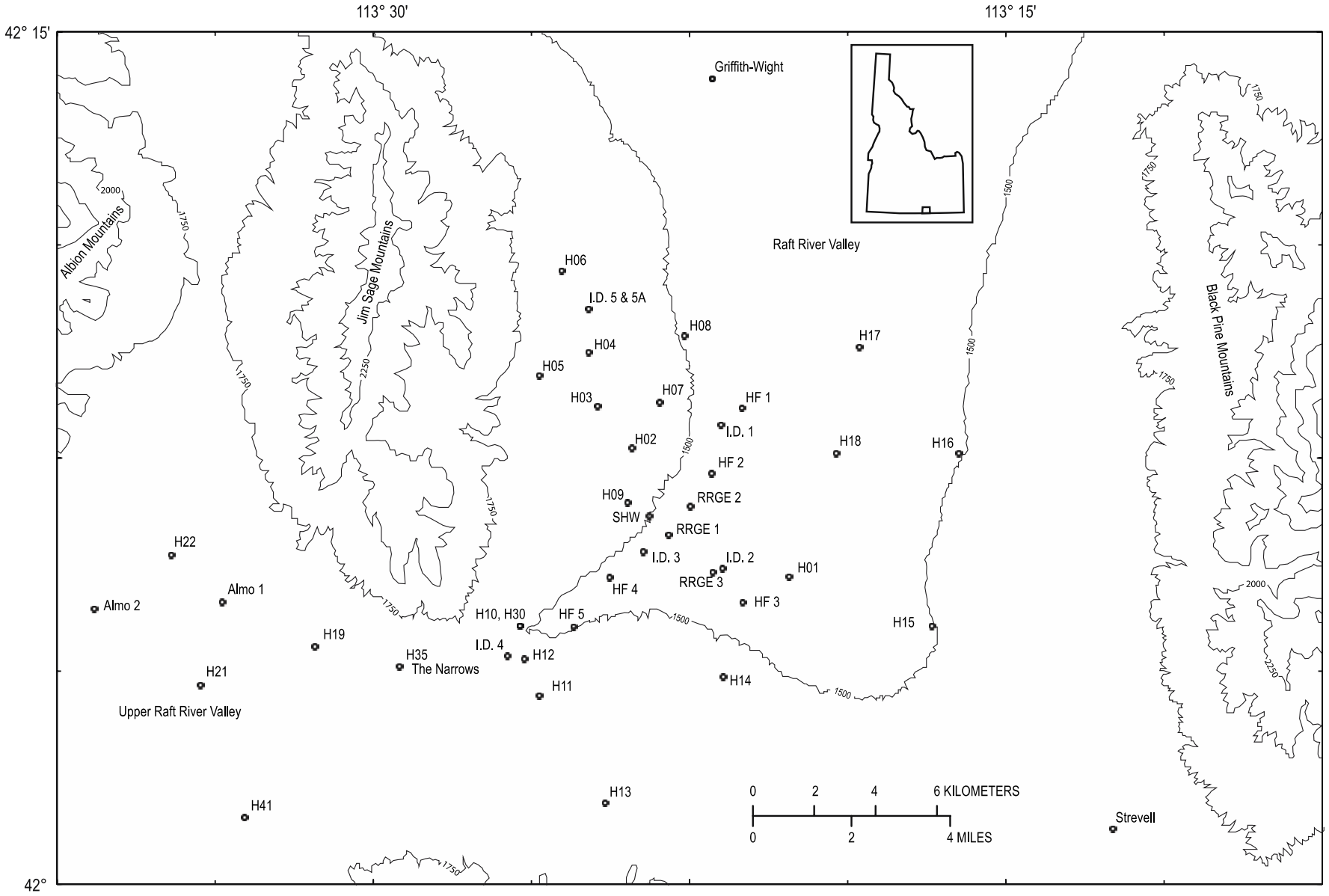

Figure 4. Map showing locations for drill holes reported in this study, Raft River Valley, Idaho. Elevation contours in meters. Inset shows map of Idaho with an outline of the area shown in the figure.

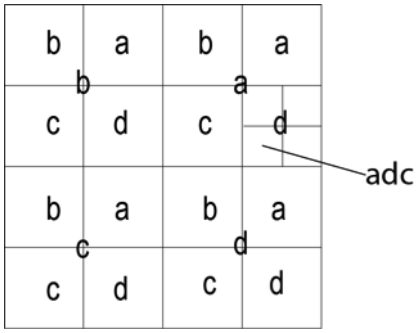

Figure 5. Diagram of letter codes designating parts of sections for the location data given in table 1.

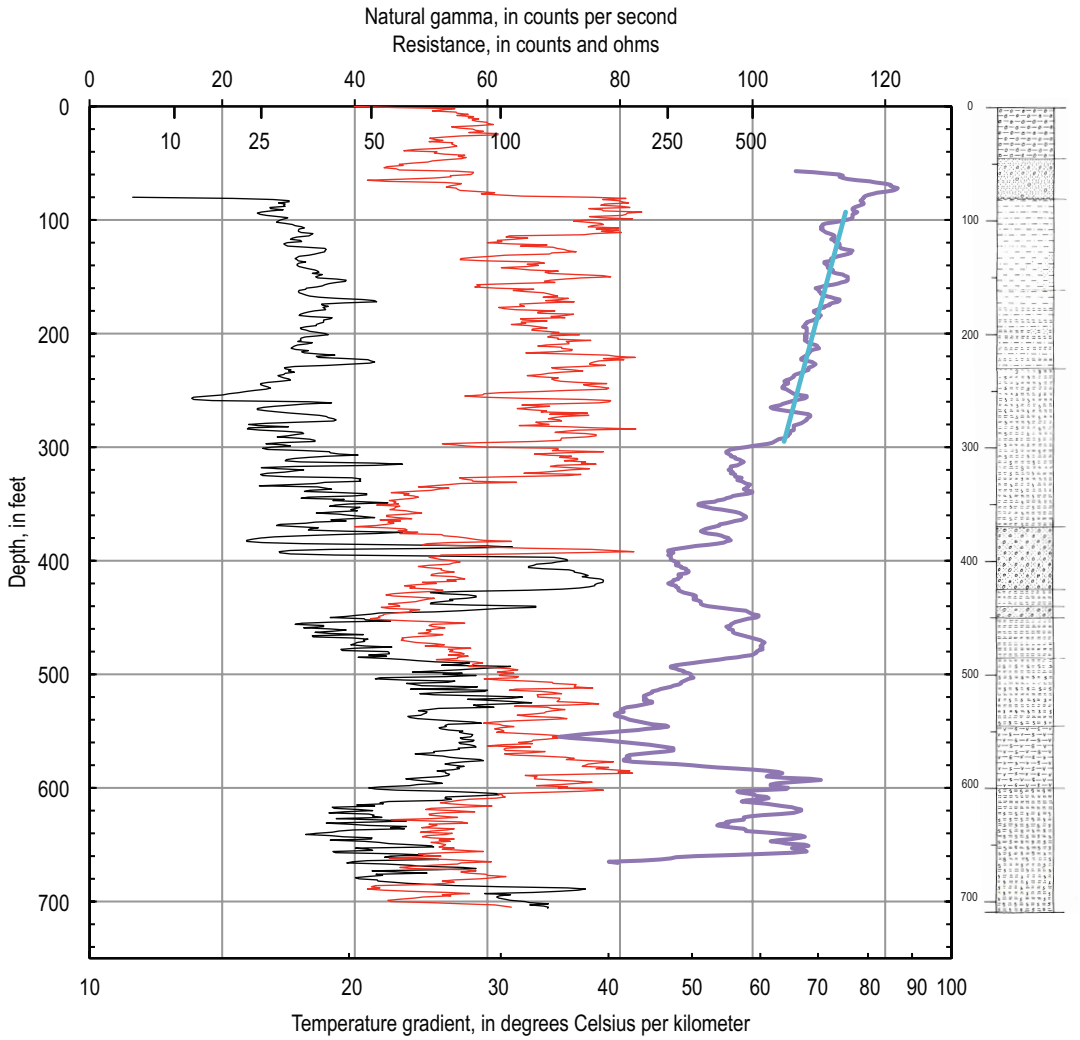

FAN ALLUVIUM

0–45 ft Gravel in a tan, calcareous silt matrix. Gravel: subrounded clasts of gray and black rhyolite lava as much as 3 cm in diameter

45–80 f t Sand and gravel in a tan silt matrix. Sand: coarse, angular grains of red and gray rhyolite lava. Gravel: subangular clasts of red and gray rhyolite lava as much as 2 cm in diameter

SALT LAKE FORMATION

80–160 ft Siltstone: salmon-colored, calcareous; sandy below 130 ft, with medium sand grains of gray rhyolite lava and green secondary silica

160–230 ft Claystone and siltstone in alternating laminae; salmon-colored, very hard

230–370 ft Claystone: alternating light green and salmon-colored laminae, very hard; appears partly silicified in places. Below 310 ft light green laminae change to dark gray and become slightly calcareous

370–425 ft Conglomerate: subangular to subrounded clasts of quartz monzonite and minor quartzite as much as 10 cm in diameter in a clean quartz sand matrix. Sand: subangular to rounded and fine to medium grained

425–440 ft Claystone: light and dark gray laminae, micaceous, calcareous

440–450 ft Conglomerate: subangular to subrounded clasts of quartz monzonite and minor quartzite as much as 10 cm in diameter in a clean quartz sand matrix

450–485 ft Claystone: light and dark gray laminae, micaceous, calcareous

485–545 ft Claystone: alternating beds of light gray, micaceous and calcareous claystone and dark gray silicified claystone

545–600 ft Siltstone: light green, tuffaceous, partly silicified

600–709 ft Claystone: alternating beds and laminae of light gray calcareous claystone and dark gray silicified claystone. Dark gray silicified claystone is brecciated in places and is within the light-gray claystone

EXPLANATION
Resistance 10/2/77
Natural gamma 10/3/77
Gradient
Flow model

Figure 6. Lithologic columnar section and geophysical logs for well H04. Natural gamma-ray (in counts per second) and resistance (in counts) shown on the same top scale with resistance values (in ohms) shown on the scale within the plot area. Temperature gradient data are shown with the bottom (log) scale and are calculated over 10-foot intervals with the value plotted near the mid-point of the interval. Straight-line match to the natural log of the temperature gradient is shown. See figure A-1 for lithology symbol key. For Salt Lake Formation see Williams and others (1982).

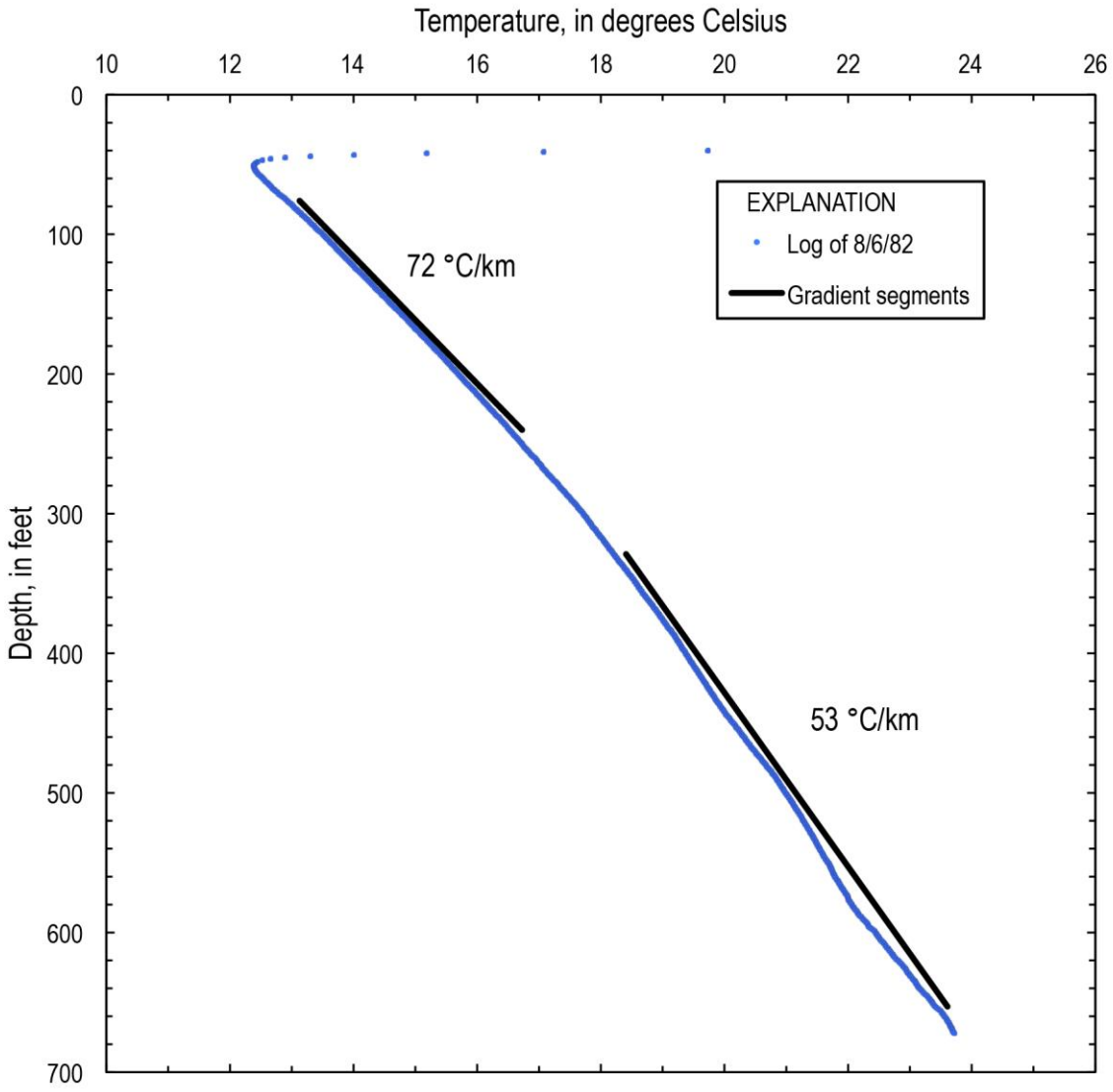

Figure 7. Graph of temperature versus depth for well H04. Straight lines for calculating temperature gradients are shown over intervals chosen by eye, and the lines are displaced from the data by 0.2 °C for clarity.

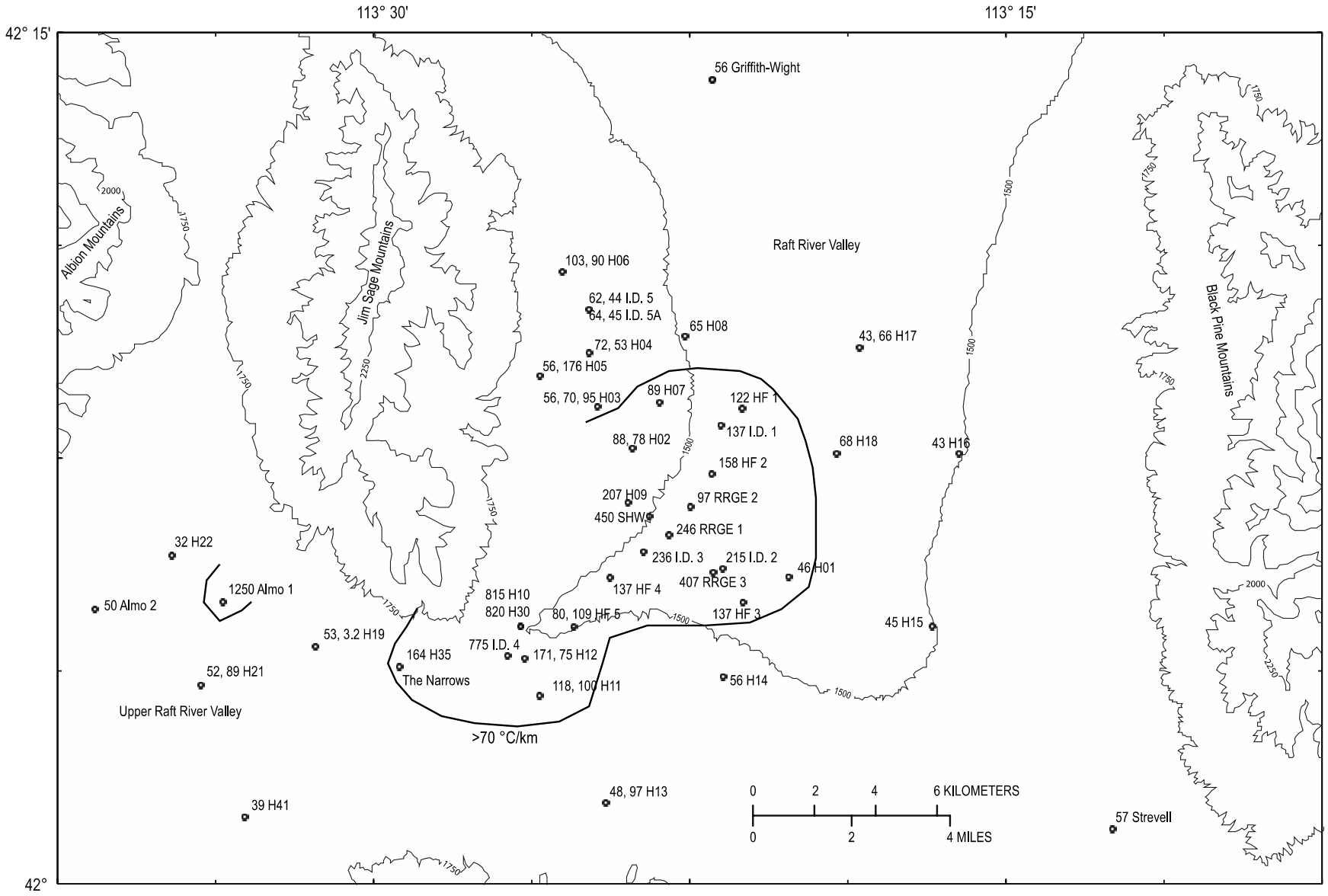

Figure 8. Map of locations of drill holes along with representative temperature gradients (in °C/km) listed before well name (for some wells, two gradients are for different depth intervals), Raft River Valley, Idaho. Outline of identified geothermal anomalies with temperature gradient >70 °C/km shown. Elevation contours in meters.

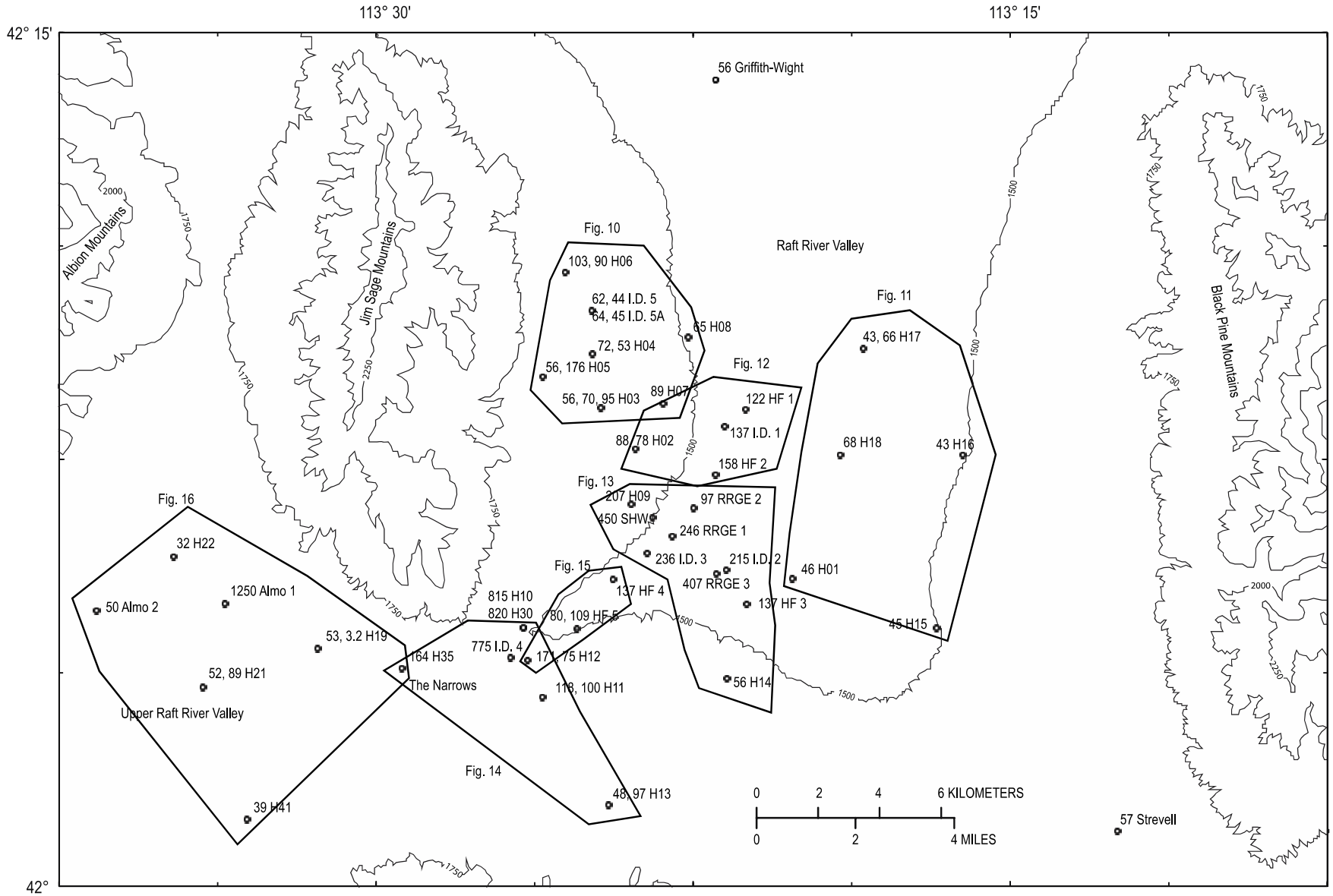

Figure 9. Map of locations of drill holes in Raft River Valley, Idaho, showing areas for plots of temperature versus depth (figs. 10–16) along with representative temperature gradients (for some wells, two gradients are for different depth intervals). Where areas overlap, data for that drill hole are shown on both plots. Elevation contours in meters.

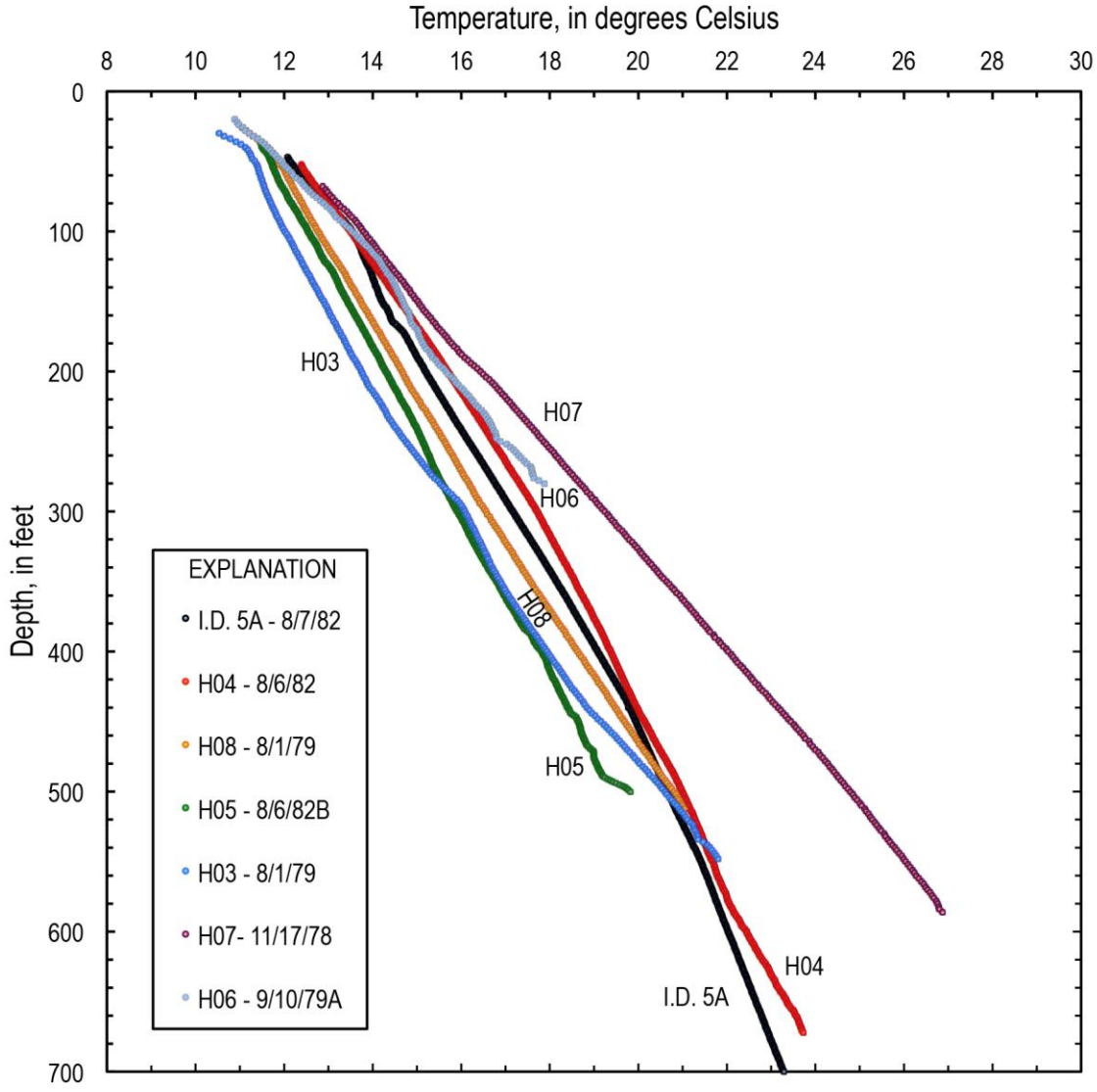

Figure 10. Graph of temperature versus depth for drill holes in the northwest part of the Raft River Valley. Dates of logging in m/d/yy format.

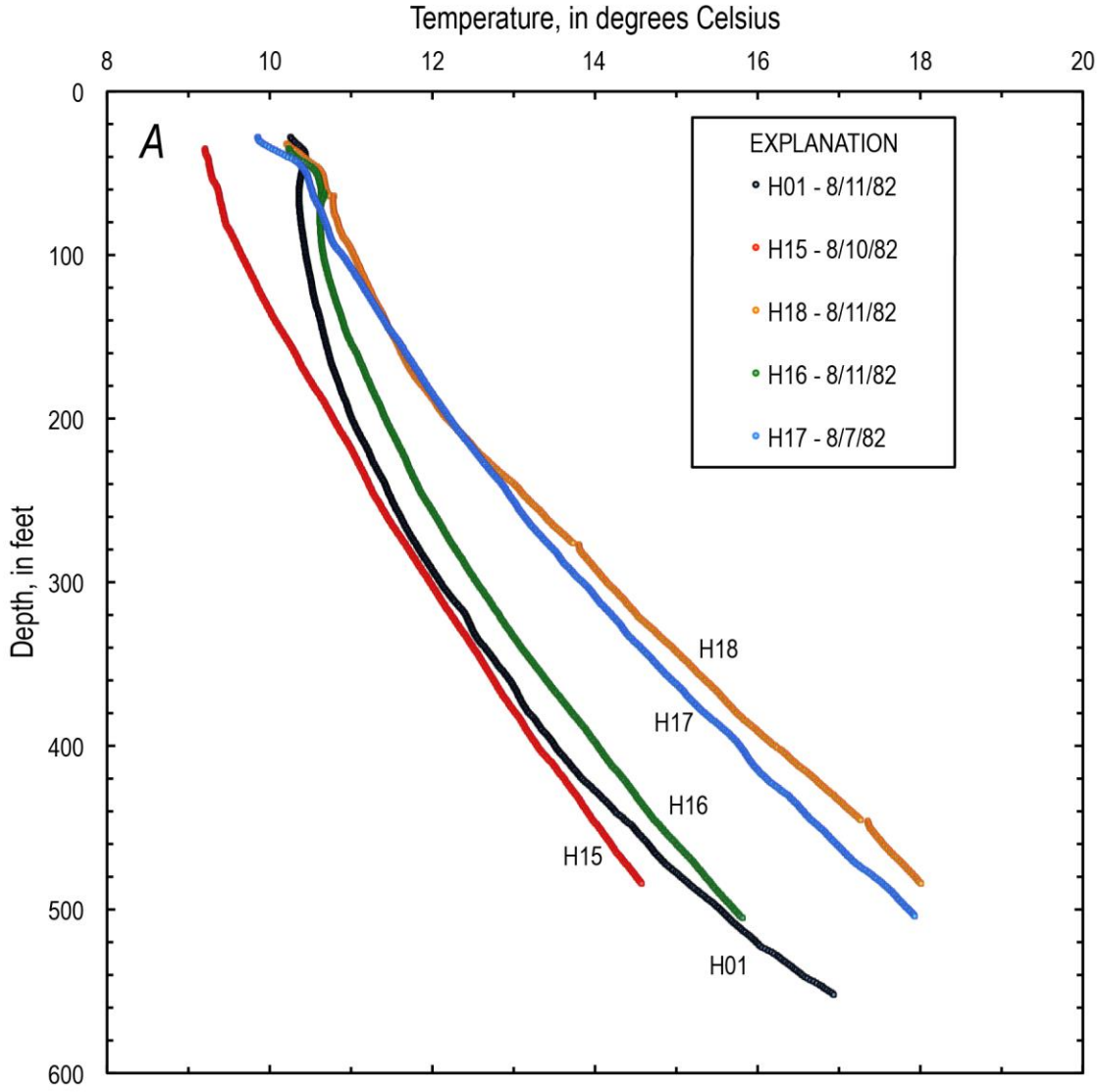

Figure 11. Data for drill holes in the eastern part of the Raft River Valley. Dates of logging in m/d/yy format. *A*, Graph of temperature versus depth. *B*, Graph of temperature versus depth and temperature gradients (note log scale) for drill holes H01 and H16. Temperature gradient data are shown with the bottom (log) scale and are calculated over 10-foot intervals with the value plotted near the mid-point of the interval. Straight-line matches to the natural log of the temperature gradient are shown for model for vertical flow of water.

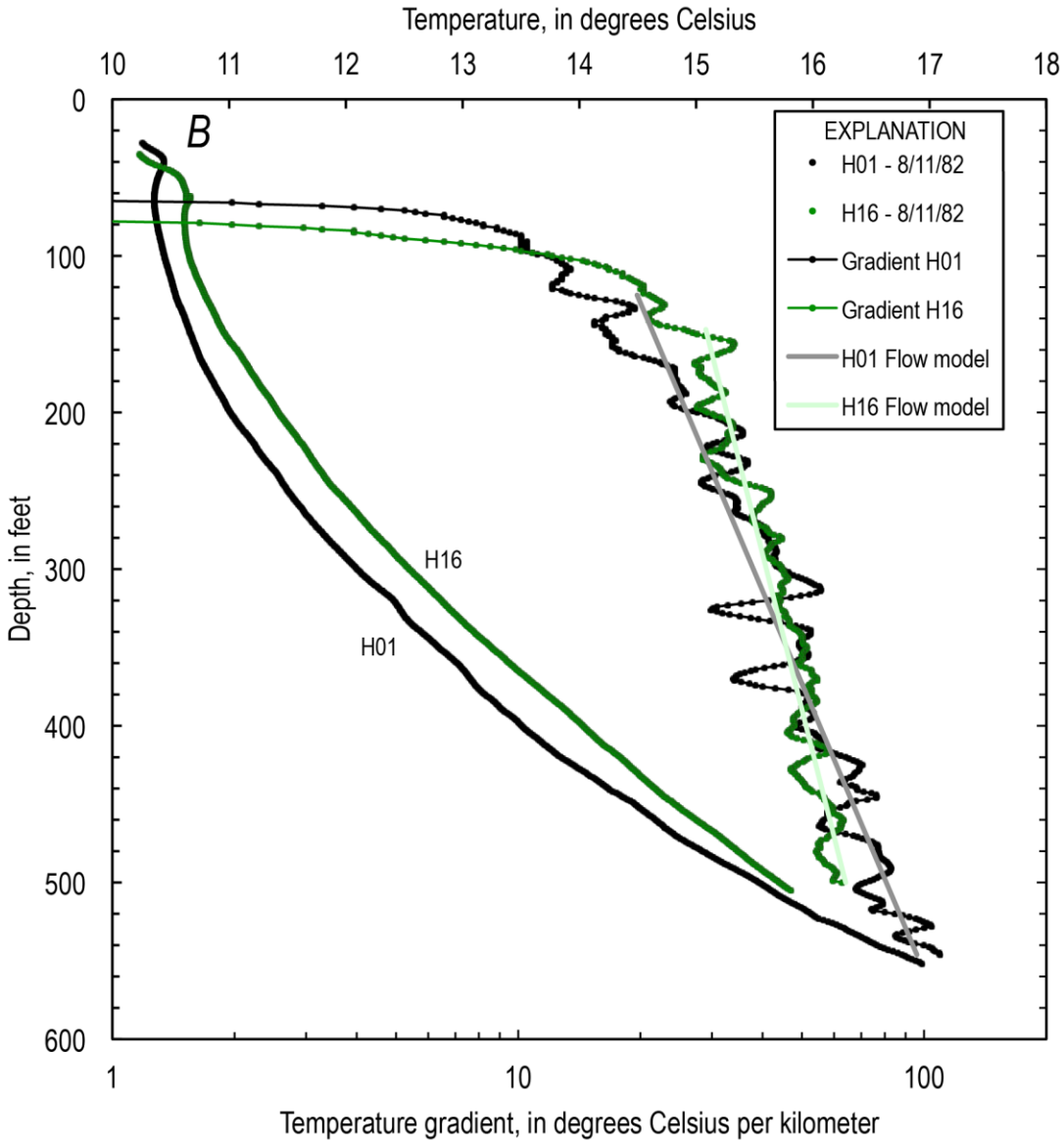

Figure 11.—Continued

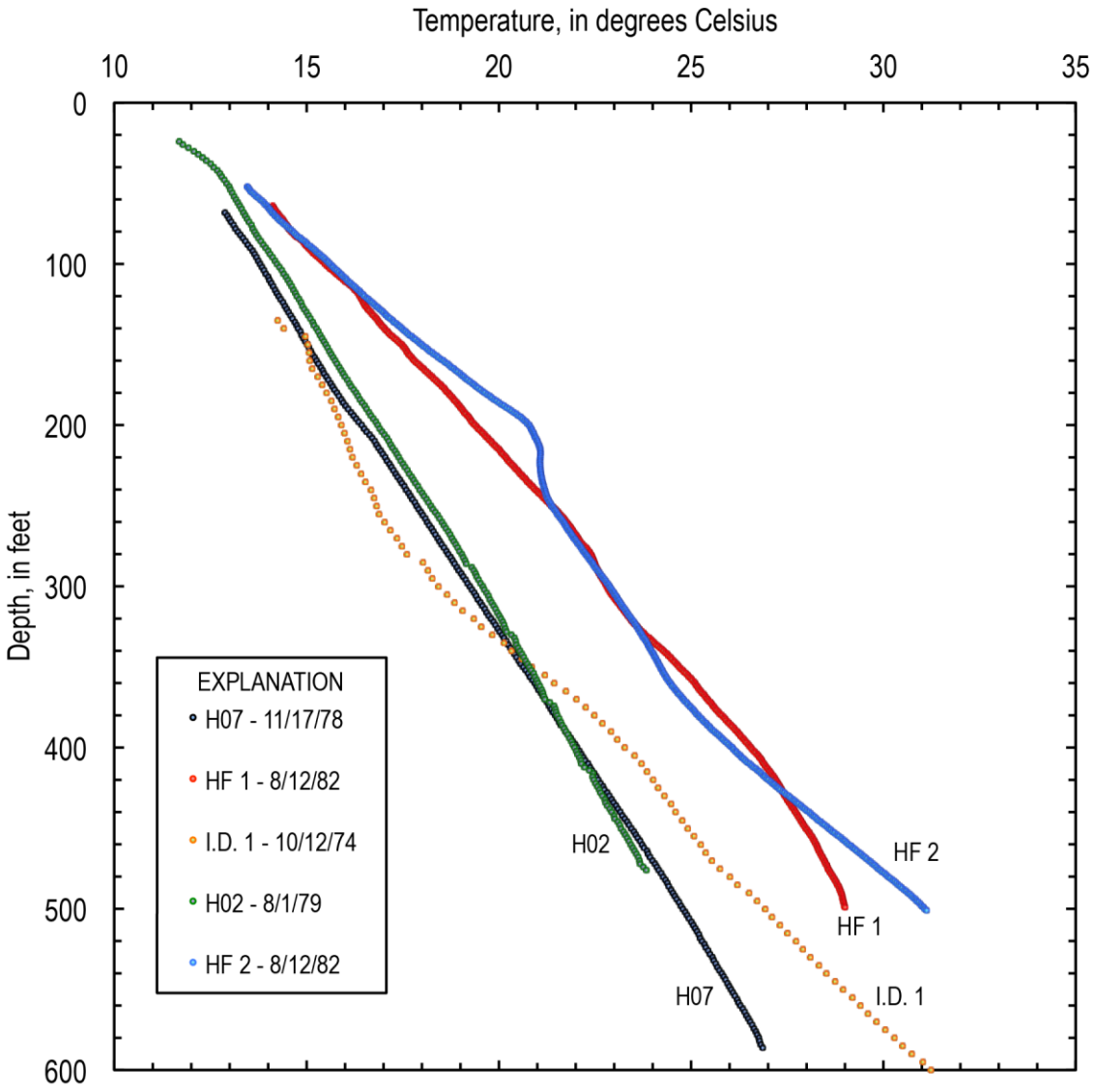

Figure 12. Graph of temperature versus depth for drill holes north of the deep well area, Raft River Valley. Dates of logging in m/d/yy format.

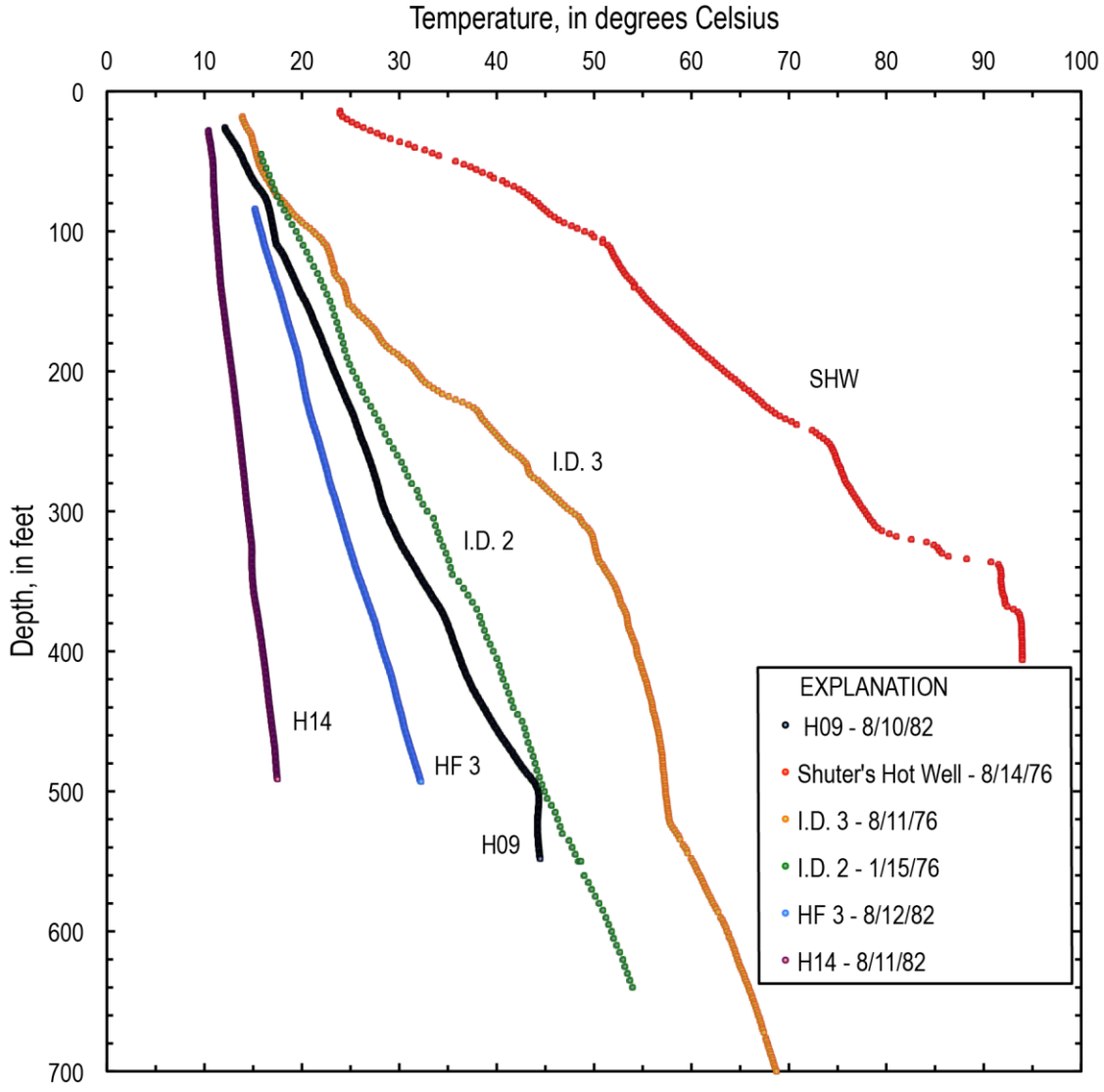

Figure 13. Graph of temperature versus depth for drill holes in the deep well area, Raft River Valley. Dates of logging in m/d/yy format.

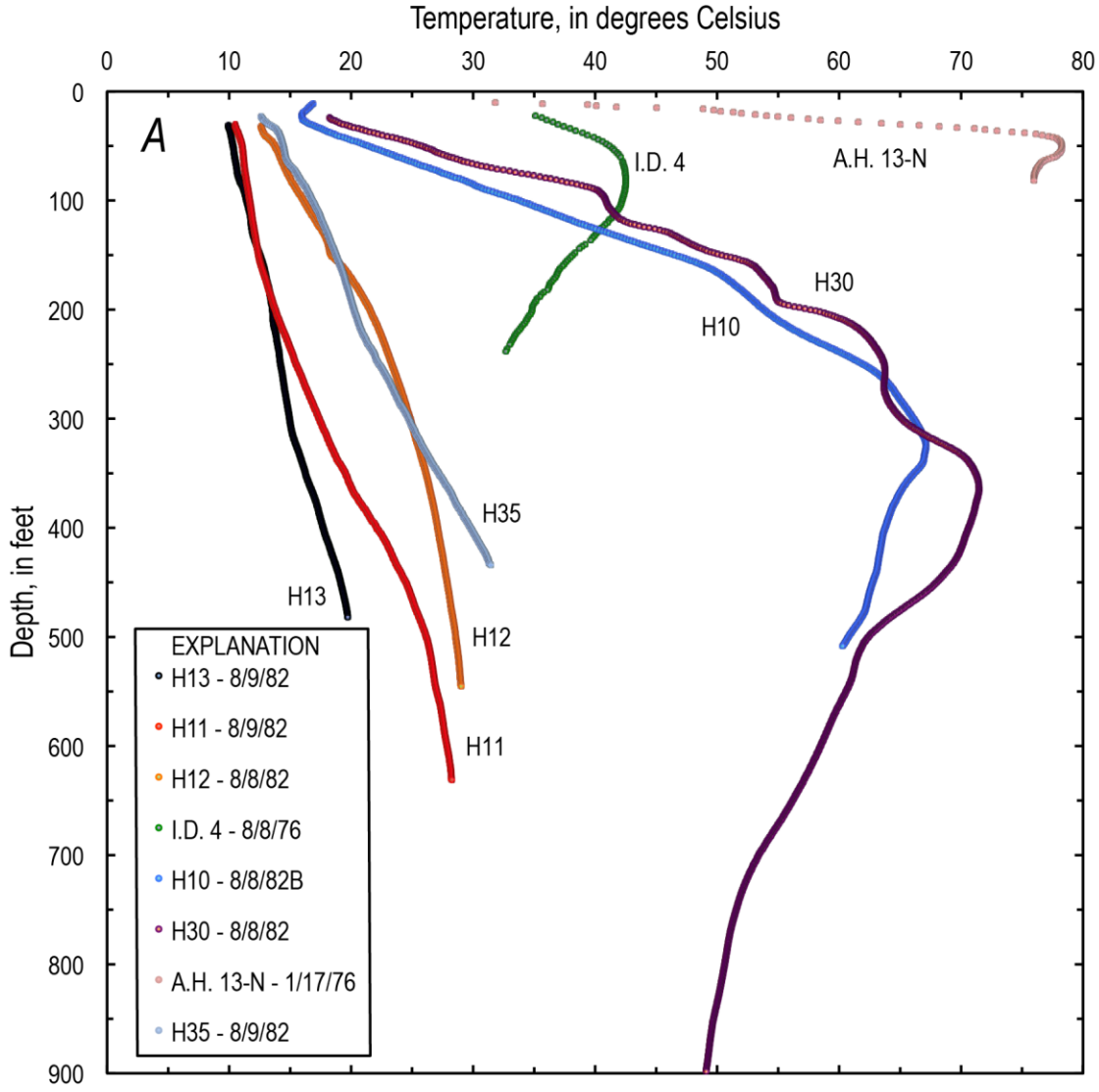

Figure 14. Data for wells in the Narrows area, Raft River Valley. Dates of logging in m/d/yy format. *A*, Graph of temperature versus depth. *B*, Graph of temperature versus depth with expanded scales and temperature gradient for selected drill holes in The Narrows area. Temperature gradient data are shown with the bottom (log) scale and are calculated over 10-foot intervals with the value plotted near the mid-point of the interval. Straight-line matches to the natural log of the temperature gradient are shown for model for vertical flow of water.

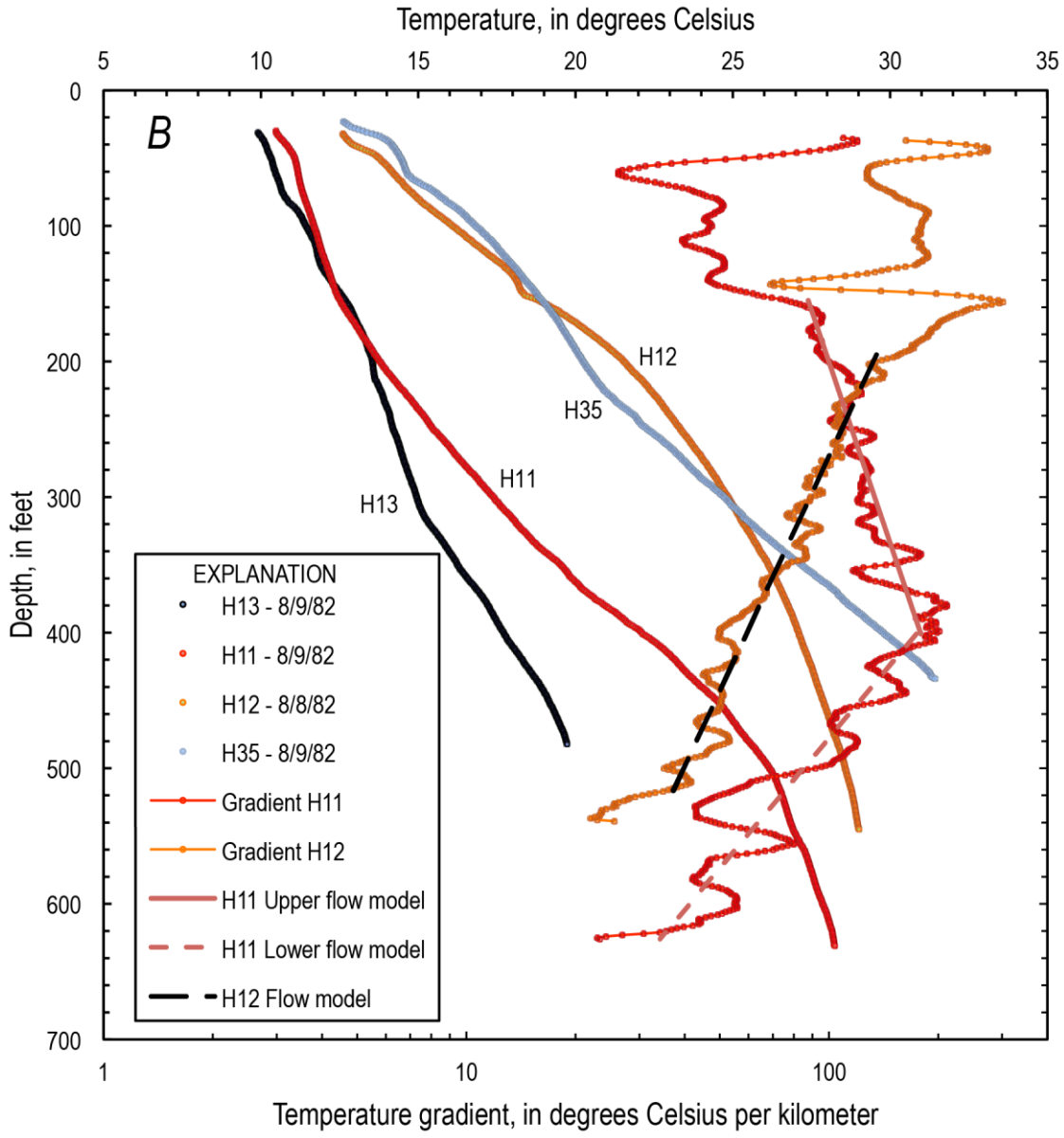

Figure 14.—Continued

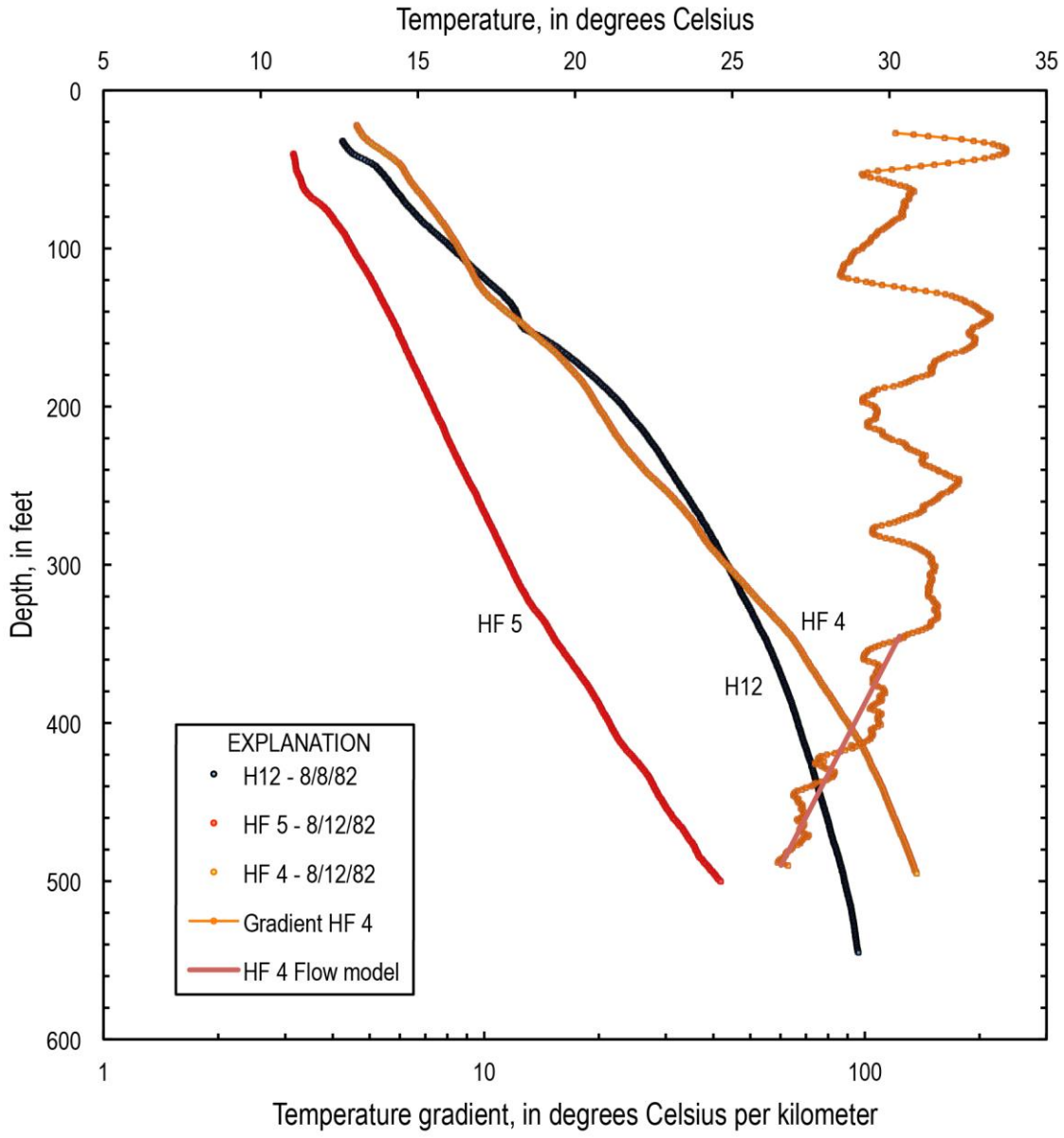

Figure 15. Graph of temperature versus depth and temperature gradient for drill holes between The Narrows and deep well areas. Temperature gradient data are shown with the bottom (log) scale and are calculated over 10-foot intervals with the value plotted near the mid-point of the interval. Straight-line match to the natural log of the temperature gradient is shown for model for vertical flow of water. Dates of logging in m/d/yy format.

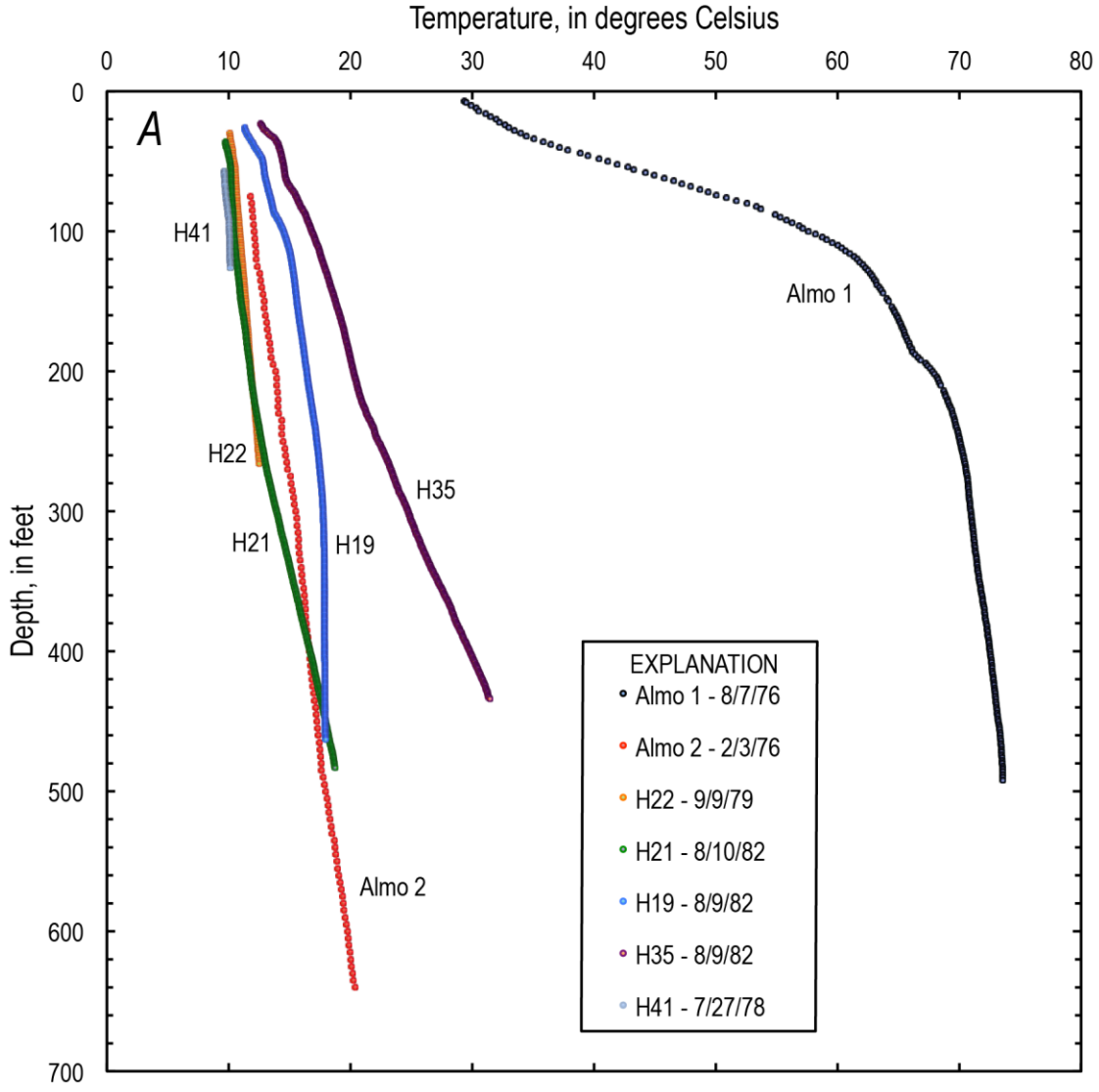

Figure 16. Data for wells in the Upper Raft River Valley. Dates of logging in m/d/yy format. *A*, Graph of temperature versus depth for drill holes. *B*, Graph of temperature versus depth for drill holes in the Upper Raft River Valley on an expanded scale, without data for Almo 1.

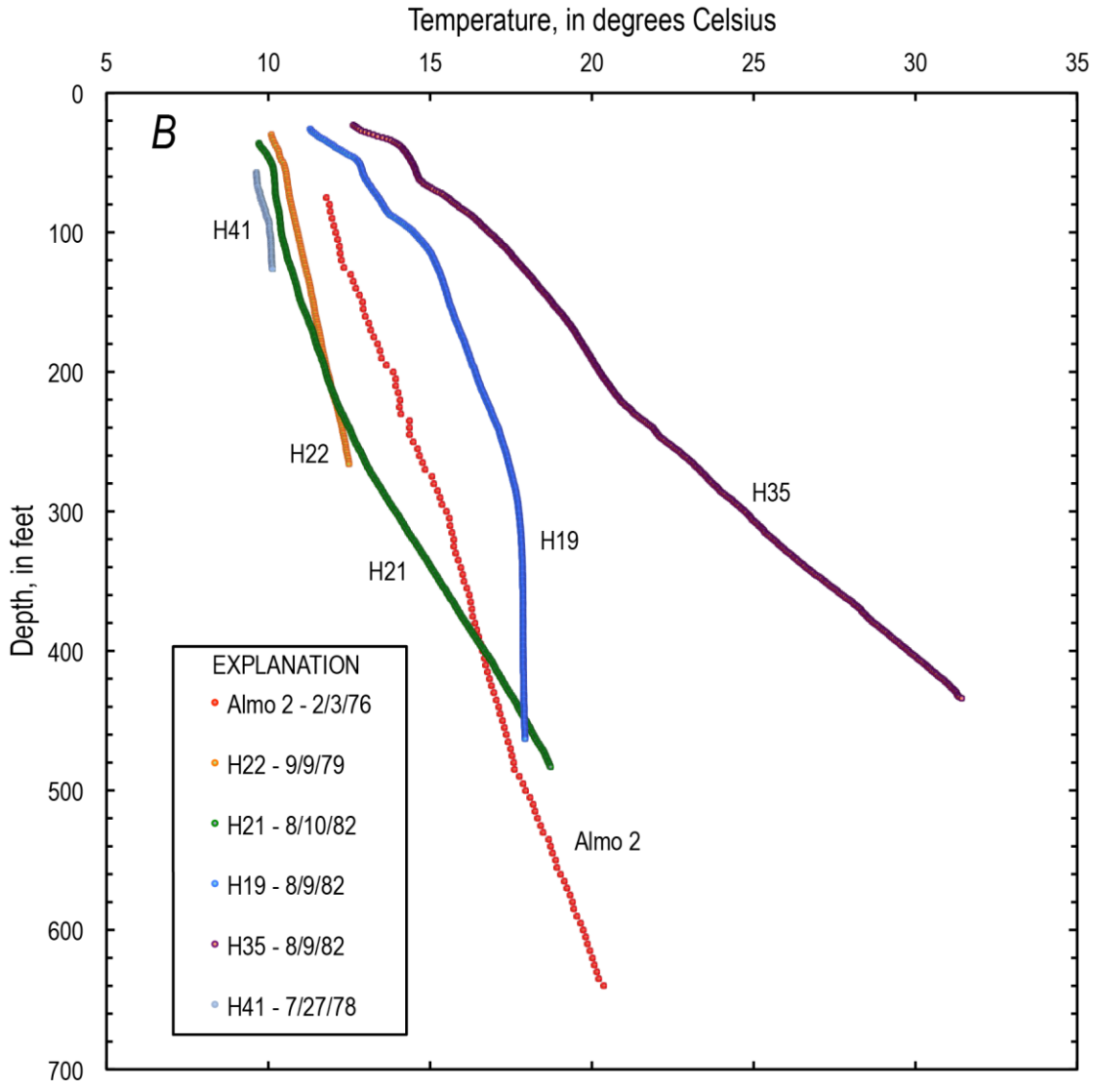

Figure 16.—Continued

Table 1. Locations of drill holes reported in this study.

[Drilled dates (m/d/yy format) and cased depths given for wells drilled as part of this study; TD, total depth. T.R.S. is Township, Range, and Section as given on USGS topographic maps. Letter codes for parts of sections explained in figure 5. Locations use North American Datum of 1927]

Name	T. R. S.	Latitude	Longitude	Elevation (ft)	Drilled dates	Cased depth (ft)
Griffith-Wight	14S-26E-1bdb	42°14.17'	113°21.97'	4,630		
H06	14S-26E-28bac	42°10.79'	113°25.53'	5,435	9/14/77	80 (320 TD)
I.D. 5A	14S-26E-33aab	42°10.12'	113°24.90'	5,240		
H04	14S-26E-33ddc	42°09.36'	113°24.89'	5,260	9/6/77-10/3/77	705
H08	14S-26E-35dab	42°09.65'	113°22.62'	4,900	9/16/77–9/20/77	515
H17	14S-27E-33cdb	42°09.45'	113°18.48'	4,700	12/5/77–12/17/77	504
Almo 2	15S-24E-35aab	42°04.84'	113°36.62'	5,240		
Almo 1	15S-25E-29cdd	42°04.97'	113°33.58'	5,140		
H22	15S-25E-30baa	42°05.79'	113°34.79'	5,180	1/7/78–1/9/78	268
H19	15S-25E-34cdb	42°04.18'	113°31.39'	5,080	12/20/77–1/7/78	463
H07	15S-26E-2cdc	42°08.48'	113°23.22'	5,020	9/15/77–9/28/77	596
H03	15S-26E-3ccc	42°08.41'	113°24.69'	5,240	9/2/77–9/4/77	558
H05	15S-26E-5adb	42°08.95'	113°26.06'	5,500	9/14/77–10/12/77	508
H02	15S-26E-10dca	42°07.68'	113°23.87'	5,060	8/21/77–8/22/77	496
HF 1	15S-26E-12aaa	42°08.38'	113°21.26'	4,790		
I.D. 1	15S-26E-12acb	42°08.08'	113°21.76'	4,850		
HF 2	15S-26E-13bdc	42°07.23'	113°21.98'	4,840		
H09	15S-26E-15dcc	42°06.72'	113°23.97'	5,020	10/13/77-10/15/77	548
I.D. 3	15S-26E-22ddd	42°05.85'	113°23.60'	4,860		
RRGE 2	15S-26E-23aaa	42°06.65'	113°22.49'	4,840		
SHW	15S-26E-23bbc	42°06.48'	113°23.46'	4,924		
RRGE 1	15S-26E-23caa	42°06.15'	113°23.00'	4,840		
I.D. 2	15S-26E-25acb	42°05.56'	113°21.72'	4,840		
RRGE 3	15S-26E-25bdc	42°05.49'	113°21.95'	4,850		
HF 3	15S-26E-25ddd	42°04.96'	113°21.24'	4,860		
HF 4	15S-26E-27bdc	42°05.40'	113°24.40'	4,880		
H10	15S-26E-32bdd	42°04.54'	113°26.52'	4,960	10/17/77–10/28/77	508
H30	15S-26E-32bdd	42°04.54'	113°26.52'	4,960	11/7/77–11/14/77	900
HF 5	15S-26E-33acc	42°04.53'	113°25.25'	4,920		
H18	15S-27E-8ddc	42°07.58'	113°19.02'	4,750	?–12/20/77	484
H16	15S-27E-11cdc	42°07.58'	113°16.12'	4,910	12/4/77–12/14/77	505
H01	15S-27E-30adc	42°05.41'	113°20.15'	4,810	8/29/77–8/31/77	558
H15	15S-27E-34adc	42°04.54'	113°16.75'	4,910	11/18/77–12/15/77	484
H21	16S-25E-8bcc	42°03.50'	113°34.10'	5,180	1/4/78–1/8/78	483
H35	16S-25E-12bbc	42°03.83'	113°29.39'	5,040	1/10/78–1/15/78	433
H41	16S-25E-29aad	42°01.18'	113°33.06'	5,400	1/11/78–1/17/78	80 (126 TD)
H14	16S-26E-1acc	42°03.65'	113°21.71'	4,980	11/17/77–12/6/77	490
H12	16S-26E-5abb	42°03.97'	113°26.42'	5,000	11/30/77–12/2/77	545
I.D. 4	16S-26E-5bba	42°04.02'	113°26.82'	4,960		
H11	16S-26E-5ddb	42°03.32'	113°26.07'	5,100	10/30/77–11/2/77	634
H13	16S-26E-15ccd	42°01.43'	113°24.50'	5,380	1116/77–12/3/77	482
Strevell	16S-28E-20cac	42°00.97'	113°12.47'	5,280		

Table 2. Calculated vertical velocities from flow model.

[Positive velocity is downward. Thermal conductivity value of 1.3 watt meter^{-1} °C^{-1}. Coefficient of determination r^2 given for each fit]

Well ID	Depth range (ft)	Velocity (m/y)	r^2
H01	125–546	0.12	0.90
H04	93–295	-0.026	0.77
H11	155–401	0.094	0.82
H11	401–626	-0.23	0.83
H12	195–517	-0.13	0.96
H16	147–500	0.072	0.88
HF4	345–490	-0.16	0.87

Table 3. Thermal conductivites, temperature gradients, and heat flow for wells at Raft River, Idaho.

[Thermal conductivity in watts meter^{-1} °C^{-1}. Heat flow in milliwatts meter^{-2}]

Well ID	Depth range (ft)	Thermal conductivity (W m^{-1} °C^{-1})	Standard deviation (W m^{-1} °C^{-1})	Depth range (ft)	Gradient (°C/km)	Heat flow (mW/m^2)
I.D. 1	293–1100	1.08	0.15	345–605	136.7	148
I.D. 2	257–786	1.30	0.29	75–590	214.9	279
I.D. 3	212–1328	1.68	0.43	116–884	235.9	396
I.D. 5	114–392	1.87	0.23	189–395	61.9	116
	405–658	2.38	0.36	500–716	44.2	105
	114–658	2.10	0.39			

Table 4. Representative temperature gradients for wells at Raft River, Idaho.
[Depths and temperatures used to calculate gradients are given]

Well ID	Depth (ft)	Temperature (°C)	Depth (ft)	Temperature (°C)	Gradient (°C/km)
SHW	106	50.859	312	79.12	450.1
I.D. 1	345	20.605	605	31.441	136.7
I.D. 2	75	17.481	590	51.213	214.9
I.D. 3	116	22.861	884	78.086	235.9
I.D. 4	24	35.618	42	39.867	774.5
I.D. 5	189	15.078	395	18.967	61.9
	500	20.614	716	23.523	44.2
I.D. 5A	165	14.474	407	19.213	64.3
	500	20.668	1194	30.163	44.9
Strevell	215	13.147	685	21.242	56.5
Almo 1	36	35.824	82	53.305	1246.9
Almo 2	155	12.921	630	20.145	49.9
Griffith-Wight	655	33.167	1285	43.863	55.7
	4260	85.001	4710	92.359	53.6
RRGE 1	325	53.334	630	76.188	245.8
RRGE 2	289	54.339	1072	77.41	96.7
RRGE 3	310	45.13	480	66.192	406.5
HF1	79	14.569	415	27.05	121.9
HF2	57	13.641	172	19.186	158.2
HF3	91	15.439	484	31.816	136.7
HF4	44	14.263	340	26.659	137.4
HF5	122	13.587	308	18.116	79.9
	333	18.923	482	23.888	109.3
H01	62	10.36	143	10.637	11.2
	483	15.124	515	15.873	76.8
	80	10.384	552	16.934	45.5
H02	60	13.166	252	18.286	87.5
	288	19.29	472	23.673	78.2
H03	80	11.703	210	13.904	55.5
	348	16.846	420	18.371	69.5
	440	18.835	508	20.81	95.3
H04	76	12.928	240	16.526	72.0
	329	18.209	653	23.409	52.7
H05	58	11.802	480	19.053	56.4
	488	19.181	500	19.823	175.5

Well ID	Depth (ft)	Temperature (°C)	Depth (ft)	Temperature (°C)	Gradient (°C/km)
H06	36	11.497	116	14.016	103.3
	184	15.219	264	17.424	90.4
H07	88	13.472	560	26.277	89.0
H08	90	12.579	462	19.946	65.0
H09	118	18.173	227	25.038	206.6
H10	29	16.486	150	46.544	815.0
H11	183	13.288	334	18.713	117.9
	378	20.821	619	28.145	99.7
H12	58	14.095	171	19.992	171.2
	199	21.496	515	28.761	75.4
H13	218	13.742	301	14.966	48.4
	322	15.423	437	18.83	97.2
	86	11.056	464	19.439	72.8
H14	140	11.702	314	14.687	56.3
H15	248	11.299	448	14.018	44.6
H16	146	10.934	245	11.857	30.6
	324	12.87	498	15.679	53.0
	122	10.776	505	15.812	43.1
H17	103	10.938	201	12.227	43.2
	302	13.89	487	17.605	65.9
H18	210	12.371	470	17.744	67.8
H19	145	15.529	222	16.772	53.0
	311	17.789	463	17.935	3.2
H21	122	10.645	246	12.61	52.0
	261	12.928	405	16.838	89.1
H22	88	10.787	236	12.241	32.2
H30	45	24.377	152	51.114	819.9
H35	244	22.007	413	30.454	164.0
H41	62	9.644	90	9.976	38.9

Menlo Park Publishing Service Center, California
Manuscript approved for publication September 12, 2014
Text edited by Peter H. Stauffer
Design and layout by Cory D. Hurd